Origin of Internal Viscosity Effects in Flexible Polymers: A Comparative Neutron Spin-Echo and Light Scattering Study on Poly(dimethylsiloxane) and Polyisobutylene

A. Arbe,[†] M. Monkenbusch,[‡] J. Stellbrink,[‡] D. Richter,*[,‡] B. Farago,[§] K. Almdal,[⊥] and R. Faust[#]

Departamento de Física de Materiales, Universidad del País Vasco, and Unidad de Física de Materiales (CSIC-UPV/EHU), Apartado 1072, 20080 San Sebastián, Spain; Institut für Festkörperforschung, Forschungszentrum Jülich, 52425 Jülich, Germany; Institut Laue-Langevin, 156X, 38042 Grenoble Cedex, France; The Danish Polymer Centre, Condensed Matter Physics and Chemistry Department, Risø National Laboratory, DK-4000 Roskilde, Denmark; and Polymer Science Program, Department of Chemistry, University of Massachusetts−Lowell, One University Avenue, Lowell, Massachusetts 01854

Received September 21, 2000; Revised Manuscript Received December 18, 2000

ABSTRACT: We present a comparative neutron spin-echo and dynamic light scattering study of the chain dynamics of the dynamically very flexible poly(dimethylsiloxane) (PDMS) with the orientationally hindered polyisobutylene (PIB). Both polymers exhibit the same static rigidity. In the melt PDMS follows the Rouse dynamics up to momentum transfers of $Q = 0.4$ Å^{-1}, while PIB displays a strong influence of local dynamics already above $Q = 0.15$ Å^{-1}. In dilute solution the dynamic structure factors and the diffusion coefficients of both polymers were studied over a wide temperature and Q range. A comparative evaluation of the PIB intrachain dynamics on the basis of PDMS results, which are taken to reflect as in the melt "ideal" relaxations, shows that intrachain viscosity effects are the leading mechanism displayed by the Rouse and Zimm models. The characteristic relaxation time of the intrachain viscosity τ_0 agrees well with the rotational barriers in PIB, corroborating the underlying physical idea of a delayed redistribution of conformational states to be at the origin of internal viscosity effects.

I. Introduction

The large-scale motions in homopolymer melts and solutions are largely determined by chain connectivity effects or entropy and in solutions additionally by hydrodynamic interactions.[1,2] In a length scale regime where topological interactions are not yet important, in polymer melts the Rouse model[3] has been particularly successful. This model considers the conformational entropy as the only source of restoring forces stabilizing excursions from equilibrium. At shorter length scales where the simplifying assumptions of the Rouse model do not hold, the influence of the local chain structure becomes important. Both local stiffness and rotational potentials begin to play a role.[4,5] Recently, by neutron spin-echo spectroscopy we have investigated thoroughly the transition from entropic Rouse motion to local chain dynamics on polyisobutylene (PIB) melts and scrutinized different models for this dynamic regime.[6] The outcome was as follows:

(i) The experiments demonstrated that for a flexible polymer the remaining chain stiffness does not explain the observed spectra.

(ii) The observed significant slowing down of the relaxation at larger momentum transfers Q (or shorter distances) compared to the Rouse prediction invokes the presence of extra dissipation effects. The intrachain viscosity model of Allegra et al.[4,5] describes such dissipation as due to a delayed redistribution of local conformations following fluctuations from equilibrium. With the characteristic time τ_0 for this process as the only parameter, the model was able to successfully describe all spectra that were observed over a wide Q range.

(iii) The local relaxation time τ_0, however, displayed no obvious connection to the intrachain rotational potential of PIB, signifying some unspecified influence of the embedding melt.

To more deeply understand the leading mechanism coming into play upon leaving the universal regimes, we studied the same PIB molecule now in dilute toluene solution. Thereby we covered a wide temperature range. In dilute solution interchain friction effects are weak, and the nature of the intrachain relaxation parameter τ_0 should reveal itself.

Complicating the interpretation, on the other hand, the dynamics of polymers in solution is affected by the hydrodynamic interaction between different moving entities.[4,5,7] Since the description of this interaction within the Rouse−Zimm model is only well proven in the long wavelength limit and has its shortcomings at higher wavenumbers, we take a comparative approach. We compare the dynamics of PIB which exhibits a high rotational barrier[8−12] with that of poly(dimethylsiloxane) (PDMS), a polymer with nearly no internal barriers.[13] Thereby we use chains of practical identical chain dimensions and identical translational diffusion coefficients. The comparative treatment greatly reduces the uncertainties involved in a proper treatment of the hydrodynamic interaction and allows to elucidate the nature of the intrachain viscosity effect proposed originally by Allegra et al.

The paper is structured as follows: In a theory section we (i) briefly refer to the Rouse−Zimm model and emphasize the full treatment of the hydrodynamic sums

[†] Universidad del País Vasco.
[‡] Institut für Festkörperforschung.
[§] Institut Laue-Langevin.
[⊥] Risø National Laboratory.
[#] University of Massachusetts−Lowell.

10.1021/ma001628x CCC: $20.00
Published on Web 01/31/2001

for higher modes, (ii) the main ingredients of the intrachain viscosity approach are shortly discussed, and (iii) finally we address the diffusion coefficients playing a role in the interpretation of the data. In the experimental section we present the synthesis and characterization of the PIB and PDMS samples as well as the neutron and light scattering experiments. In the results section we first present the results on the diffusion coefficient obtained from light scattering, then we compare the melt dynamics of PDMS and PIB, and thereafter we display the results on intrachain relaxation in PDMS and PIB solutions. In the analysis and discussion section the PIB spectra are evaluated in terms of the intrachain viscosity model. This evaluation uses as an input the information on the hydrodynamic interaction obtained from an analysis of the low barrier PDMS system. Finally we assess the outcome and summarize.

II. Theoretical Considerations

Neutron scattering experiments access the dynamic density−density correlation function on length and time scales corresponding to the segmental motions in polymer chains. The correlation function may be expressed in terms of mean-square distinct segment displacements

$$\langle[\vec{r}_m(t) - \vec{r}_n(0)]^2\rangle = R_{n,m}(t) \tag{1}$$

where $\vec{r}_m(t)$ and $\vec{r}_n(0)$ are the position vectors of segments m and n at the times t and 0, respectively; $\langle ... \rangle$ denotes the ensemble average. In Gaussian approximation the dynamic structure factor $S(Q,t)$ which is the spatial Fourier transformed of the pair correlation function may be written as

$$S(Q,t) = \frac{1}{N^2}\sum_{n,m}\exp\left\{-\frac{Q^2}{6}\langle[\vec{r}_m(t) - \vec{r}_n(0)]^2\rangle\right\} \tag{2}$$

$Q = (4\pi/\lambda)\sin\vartheta$ (λ = neutron wavelength; 2ϑ = scattering angle) is the momentum transfer during scattering. For diffusive motions the correlators $\langle[\vec{r}_m(t) - \vec{r}_n(0)]^2\rangle$ in general are calculated on the basis of Langevin equations.

In this paper we deal with the intrachain viscosity approach by Allegra[4,5] which is based on a mode description[14] of the chain structure factor and uses the Rouse−Zimm chain as an input. The appropriate Langevin equation for such a chain, where we treat the hydrodynamic interaction in terms of the preaveraged Oseen tensor, reads

$$-\vec{f}_n(t) + \zeta\frac{\partial\vec{r}_n}{\partial t} - \frac{\zeta}{6\pi\eta}\sqrt{\frac{6}{\pi}}\sum_{m\neq n}\frac{1}{|n-m|^{1/2}}\vec{f}_m(t) = \vec{F}_m(t) \tag{3}$$

$\vec{f}_n \cong (3k_BT/l^2)(\partial^2\vec{r}/\partial n^2)$ [in Allegra theory $\partial^2/\partial n^2$ is slightly modified due to a mode-dependent characteristic ratio $C(q)$][5] is the entropic force exerted by the "n"-monomer on the solvent. It is of equal magnitude and opposite sign as the corresponding intramolecular force. ζ and η are the monomeric friction coefficient and the solvent viscosity, respectively. $\vec{F}_m(t)$ is the stochastic force from the heat bath. Using Rouse normal coordinates, eq 3 is solved by Fourier transformation leading to the characteristic relaxation rates

$$\frac{1}{\tau_q} = \frac{3k_BT}{l^2\zeta(q)\,C(q)}\,4\sin^2\left(\frac{q}{2}\right);$$

$$\frac{1}{\zeta(q)} = 1 + 2B\sum_{k=1}^{N-1}\left(1 - \frac{k}{N}\right)\frac{\cos(qk)}{\sqrt{k}} \tag{4}$$

where $B = \zeta/[\pi\sqrt{6\pi}\eta l\sqrt{C(q)}]$ is the draining parameter—for Stokes friction of a bead with radius b the draining parameter becomes $B = (\sqrt{6/\pi})(b/l\sqrt{C(q)})$. l is the bond length; $C(q)$ denotes the mode-dependent characteristic ratio—in the all rotational state (ARS) model[14] $C(q)$ accounts for the local chain stiffness. In the limit $q \to 0$ $C(q) = C_\infty$ holds [C_∞ = characteristic ratio in RIS (rotational isomeric state) model[15]]. $q = (p\pi)/N$; $p = 1, 2, ..., N$; N = number of main chain bonds. For numerical purposes the sum in eq 4 is well approximated by $(\sqrt{2\pi/p})[1 - 2FresnelC(\sqrt{1.06p/\pi})]$ ($FresnelC(x) = \int_0^x\cos(\pi t^2/2)\,dt$).

Using proper random forces and the orthogonality of the Rouse normal modes for $C(q) \equiv C_\infty$, the mean-square segment displacements can be given in an analytic form

$$R_{n,m}(t) = 6Dt = |n-m|l^2C_\infty + \frac{4R_e^2}{\pi^2}\sum_q\frac{\tau_q}{\zeta(q)}\cos(qn)\cos(qm)(1 - e^{-t/\tau_q}) \tag{5}$$

where R_e is the end-to-end distance. Inserting eq 5 in eq 2 leads to the dynamic structure factor of the conventional Rouse−Zimm model. $B = 0$ in particular reveals the Rouse structure factor and for $B \neq 0$ neglecting the 1 in the second part of eq 4 the Zimm structure factors.

Toward short length scales the main limitation of the Rouse model for flexible chains appear to be local dissipative relaxation processes like orientational arrangements within one chain. Allegra et al.[4,5] introduced an internal viscosity as a result from a force arising due to a departure from configurational equilibrium. The relaxation process is described by one single relaxation rate τ_0. From an expression for the difference in free energy due to small excursions from equilibrium, an explicit expression for the internal viscosity force in terms of a memory function is derived and introduced into the Langevin eq 3 which is now solved by a decaying travelling wave

$$\tilde{x}(q,t) = \tilde{x}_0(q)\exp\left\{\left[i\omega(q) - \frac{1}{\tau(q)}\right]t\right\} \tag{6a}$$

with

$$\omega(q) + \frac{i}{\tau_q} = \frac{A(q) \mp \sqrt{A^2(q) + B(q)}}{2\zeta(q)\tau_0} \tag{6b}$$

$$A(q) = \frac{3k_BT}{l^2}\tau_0\sin(q) - i\left[\zeta(q) + \frac{24k_BT}{l^2C(q)}\tau_0\sin^2\left(\frac{q}{2}\right)\right] \tag{6c}$$

$$B(q) = 8\,\frac{12k_BT}{l^2C(q)}\,\zeta(q)\tau_0\sin^2\left(\frac{q}{2}\right) \tag{6d}$$

The eigenvalue eq 6b creates two q-dependent branches for the relaxation rate $1/\tau_q$ as well as for the propagation velocity $\omega(q)$. Figure 1 displays the q dependence of the

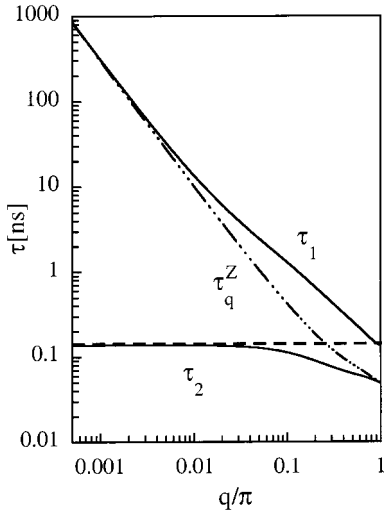

Figure 1. Mode number dependence of the relaxation times τ_1 and τ_2 (solid lines) found for PIB at 327 K. The dashed−dotted line shows the relaxation time τ_q^Z of the Rouse−Zimm model. The horizontal dashed line displays the value of τ_0.

two τ_q branches using experimental parameters taken from the later data evaluation. For comparison, also the dispersion of the Rouse−Zimm relaxation τ_q^Z without the influence of the local relaxation process is shown. For small q the Rouse−Zimm dispersion is close to the branch τ_1 while at large q τ_2 coincides with τ_q^Z. In between both modes repel each other and for small or large q reach the value of τ_0. For intermediate scale motion q values in the range below 1 are important. The main effect of the presence of the local relaxation process is a general slowing down of the chain relaxation—τ_1 bends upward!

The mean-square segment displacements which are the key ingredient for a calculation of the dynamic structure factor are obtained from a calculation of the eigenfunctions from the Langevin eq 3, including the memory function for intrachain viscosity effects. After retransformation from Fourier space to real space $R(k,t)$ ($k = |n - m|$) is given by eq 41 of ref. 4. For short chains the integral over the mode variable q has to be replaced by the appropriate sum. Finally, for observation times $t \gg \tau_0$ the mean-square displacements can be expressed in terms of eigenvalue τ_1 only. Thereby, a significant simplification of the expression for the mean-square displacements is achieved.[5]

For the proper determination of the intrachain relaxation knowledge on the overall chain translational diffusion coefficient is mandatory. We, therefore, briefly summarize the theoretical expectation for the chain diffusion coefficients keeping in mind that all experiments were performed at polymer volume fractions $\phi < \phi^*$. $\phi^* = 3M_w/(4\pi\rho N_A R_g^3)$ is the overlap volume fraction, M_w the weight-averaged molecular weight, R_g the radius of gyration ($\langle R_e^2\rangle = 6\langle R_g^2\rangle$), ρ the density, and N_A the Avogadro number. At low momentum transfers neutron and light scattering access the collective diffusion coefficient $D(\phi)$[16,17]

$$D(\phi) = D_0^\phi(1 - \phi)(1 + 2A_2V_w\phi + ...) \qquad (7)$$

with A_2 the second virial coefficient, V_w the polymer volume, and $D_0^\phi = k_BT/\zeta(\phi)$ the ϕ-dependent self-diffusion coefficient. Expanding the friction factor $\zeta(\phi)$ with respect to $\phi = 0$, $\zeta(\phi) = \zeta_0(1 + k_s^\phi\phi)$ we finally arrive at[17]

$$D(\phi) = D_0(1 - \phi)[1 + (2A_2V_w - k_s^\phi)\phi] = D_0(1 - \phi)(1 + k_D^\phi\phi) \quad (8)$$

where D_0 is the self-diffusion coefficient at infinite dilution and k_D^ϕ the "dynamic virial coefficient". At finite Q $D(\phi)$ becomes Q-dependent. The virial contribution relates to the static structure factor for interchain interactions

$$S(Q) = [1 + 2A_2V_w\phi D(QR_g)]^{-1} \qquad (9a)$$

with the Debye function

$$D(QR_g) = \frac{2}{(QR_g)^4}[\exp(-Q^2R_g^2) - 1 + Q^2R_g^2] \qquad (9b)$$

describing the scattering from a single ideal chain. Using the deGennes renormalization[18] for the structural part of the collective diffusion coefficient $D(\phi,Q) = D(\phi)/S(Q)$, the Q dependence of the virial term is directly given by $D(QR_g)$. k_s^ϕ mainly originates from the hydrodynamic interaction between chains. For its Q dependence no simple approximation besides the notion that it is governed by similar length scales as the virial part can be given.

Table 1. Parameters Characteristic for the Chains Studied in This Work

	PDMS	PIB		PDMS	PIB
M_w	6462	3870	R_g (Å)	21.3	19.2
M_w/M_n	1.10	1.06	l (Å)	1.59	1.54
N	174	138	θ (K)	240	260
C_∞	6.19	6.73			

III. Experimental Section

III.1. Samples. The poly(dimethylsiloxane) samples were prepared by anionic polymerization of hexamethylcyclotrisiloxane (D_3) in cyclohexane with *tert*-butyllithium as initiator, hexamethylphosphoric triamide (HMPA) as a polar modifier, and terminated with excess trimethylchlorosilane under inert gas conditions.[19] D_3 was obtained from Aldrich (98%). *tert*-Butyllithium was obtained from Aldrich in pentane solution. The pentane was removed on a vacuum line, and purified cyclohexane was added to produce an approximately 0.9 M solution. The exact concentration was determined through Gilman double titration. Perdeuterated D_3 was synthesized from perdeuterated methanol, CIL, 99.8% D.[20] For the hydrogenous PDMS sample 12.3 g of D_3 was initiated by 2.44 mmol of *tert*-butyllithium in 50.5 g of cyclohexane; HMPA was added such that [HMPA] = 50 mM. The polymerization ran for 22 min at 1 °C. The perdeuterated sample was prepared analogously with 7.9 g of perdeuterated D_3, 57 g of cyclohexane, and 1.47 mmol of *tert*-butyllithium and reacted for 24 min. These condition give close to quantitative conversion of the monomer to PDMS. The ratio of M_w/M_n was determined by size exclusion chromatography and is based on a polystyrene calibration curve. M_n was determined for the hydrogenous PDMS with NMR. The ratio of molar mass of the deuterious PDMS and hydrogenous was determined by SEC to be 1.06.

The details of the preparation and characterization of PIB chains can be found in ref 6. The molecular characteristics of both polymers are summarized in Table 1.

Solutions of hydrogenated chains in deuterated solvent (toluene) were prepared. The T dependence of the viscosity of protonated toluene[21] follows the Arrhenius law η_{tol} [poise] =

0.17063×10^{-3} exp(1038.9/T [K]). The values of the θ-temperatures of the solutions investigated are also included in Table 1.

For the PDMS neutron spin-echo measurements on the melt we blended protonated with deuterated PDMS chains in a 15% concentration.

III.2. Dynamic Light Scattering. Dynamic light scattering (DLS) probes the relaxation of concentration fluctuations in polymer solutions on mesoscopic time and length scales. The measured intensity autocorrelation function $g^2(Q,t) = \langle I(Q,0) I(Q,t)\rangle/\langle I\rangle^2$ is related in a homodyne experiment to the normalized field autocorrelation function $g^1(Q,t) = S(Q,t)/S(Q,0)$ by the Siegert relation: $g^2(Q,t) = 1 + f_c|g^1(q,t)|^2$ with f_c an experimental factor.[22] The intermediate scattering function $S(Q,t) = \int_V[\rho(0,0)\ \rho(\vec{r},t) - \langle\rho\rangle^2]e^{i\vec{Q}\vec{r}}\ d^3\vec{r}/\langle\rho\rangle$ is the Fourier transform of the density correlation function of the scattering medium, where $\rho(\vec{r},t)$ is the local density at position $\vec{r}$ at time t in the sample. DLS experiments were performed on an ALV SP-125 (ALV, Germany) compact goniometer in a homodyne setup using an argon ion laser (Coherent, Innova 90-4), operating with vertically polarized light at $\lambda_0 = 514.5$ nm and $I_0 = 50-800$ mW TEM_{00}. Intensity autocorrelation functions $g^2(Q,t)$ were recorded with an ALV 5000 E (fast version, 319 channels) multi-tau digital correlator covering a time window from 12.5 ns up to several hours. The scattering vector Q for light scattering is given by $(4\pi n_d/\lambda_0)$ sin ϑ, with λ_0 the wavelength in a vacuum and n_d the refractive index [n_d(toluene) = 1.494]. The experimental coherence factor f_c was determined by use of PS latex spheres (PSS, Germany) to be $f_c = 0.92$. Because of the use of a dual detector system (ALV-SO/SIPD) operating in "pseudo"-cross-correlation mode, even the first channels could be recorded without any distortion from electronic noise.

III.3. Neutron Spin Echo. The neutron spin-echo (NSE) experiments were performed by means of the spectrometer IN11 at the Institute Laue Langevin (ILL) in Grenoble. Wide Q ranges with very high-energy resolution can be explored by the NSE technique. This is achieved by coding the energy transfer in the scattering process for each neutron individually into its spin rotation. The Larmor precession of the neutron spin in an external magnetic field B_0 uses the neutron spin as an internal clock. Strongly suppressing incoherent scattering contributions, NSE measures directly the normalized intermediate scattering function $S(Q,t)/S(Q,0)$.[23] The time t depends on the wavelength λ of the neutron, the precession field B_0, and the length of the precession field L, $t \propto B_0 L \lambda^3$. Thus, the time evolution of the structure factor can be followed varying B_0. For a certain range of applicable fields, the accessible time range of the instrument can be modified by choosing a different wavelength λ, and therefore for a given Q value it is possible to explore different time windows by varying simultaneously the scattering angle 2ϑ and the selected wavelength. This allows the observation of a given process through a large Q range in the best possible dynamic interval for each Q value. In the study of the solutions we employed two different wavelengths, $\lambda = 5$ and 8 Å, and scattering angles between $2.89° \le 2\vartheta \le 18.83°$, covering a Q range: $0.04\ Å^{-1} \le Q \le 0.4\ Å^{-1}$. Using the double spin-echo setup in order to extend the study to even shorter times at 5 Å, the time interval accessed was 6 ps $\le t \le$ 25 ns. The experiments on PDMS in the bulk were performed by means of the Jülich NSE spectrometer (Forschunszentrum Jülich, Germany) ($\lambda = 8$ Å) and IN11c multidetector option of IN11- ($\lambda = 5.8$ and 7.8 Å), covering $0.04\ Å^{-1} \le Q \le 0.4\ Å^{-1}$ and an effective time range of 88 ps $\le t \le$ 22 ns.

If some protonated chains are dissolved in a deuterated matrix, the scattering intensity results from the interfering partial waves originating from the different monomers of the same chain. Thus, NSE measures the pair-correlation function for the dynamics of a single chain.[2] This dynamics can be studied in the bulk (matrix: same polymer deuterated chains) or in solution (matrix: deuterated solvent).

Our solution samples (4 mm thickness in a tight Niobium sample holder) contained 10% protonated chains. Typical measuring times were 1 h for $\lambda = 8$ Å and between 1 and 2 h for 5 Å. The background corrections are of utmost importance in this kind of experiments. If $S_{tot}(q,t)/S_{tot}(q,0)$ and $S_m(Q,t)/S_m(q,0)$ are the resulting NSE measurements on the sample and the matrix, respectively, the normalized scattering function of the chain $S(Q,t)/S(Q,0)$ is given by $S(Q,t)/S(Q,0) = A[S_{tot}(Q,t)/S_{tot}(Q,0)] + (1 - A)[S_m(Q,t)/S_m(Q,0)] = A[S_{tot}(Q,t)/S_{tot}(Q,0)] + B_g$, where $A = S_{tot}(Q,0)/[S_{tot}(Q,0) - S_m(Q,0)(T_{tot}/T_m)(1 - \phi)]$. The transmissions of both the whole sample and the matrix (T_{tot} and T_m, respectively) were measured at the employed wavelengths. The ratios obtained were $T_{tot}/T_m = 0.76$ (8 Å) and 0.83 (5 Å) for PDMS in d-toluene and 0.69 (8 Å) and 0.76 (5 Å) for PIB in d-toluene. The scattering from the matrix turned out to be time independent in the accessible instrumental time window. This elastic scattering contribution was measured for all Q values with similar statistics as the sample at three different temperatures: 220, 300, and 378 K. This allowed us to characterize its Q and T dependence—it decreased with increasing Q and T—and use interpolated values for the corrections at other temperatures. To determine the needed values of the scattering functions at $t \to 0$, we carefully measured the values of I_u (intensity of scattered neutrons not performing a spin flip in the sample) and I_d (spin flip scattering). The corrections increased with T and were important at the lowest Q values and even more important at the highest Q values [typical values at an intermediate explored T: $A(0.04\ Å^{-1}) \approx 1.12$, $A(0.10\ Å^{-1}) \approx 1.05$, $A(0.4\ Å^{-1}) \approx 1.5$; $B_g(0.04\ Å^{-1}) \approx 0.08$, $B_g(0.10\ Å^{-1}) \approx 0.01$, $B_g(0.4\ Å^{-1}) \approx 0.04$]. Because of these large corrections, the uncertainties in the amplitudes of the resulting spectra at $Q \ge 0.3\ Å^{-1}$ are of the order of 5%.

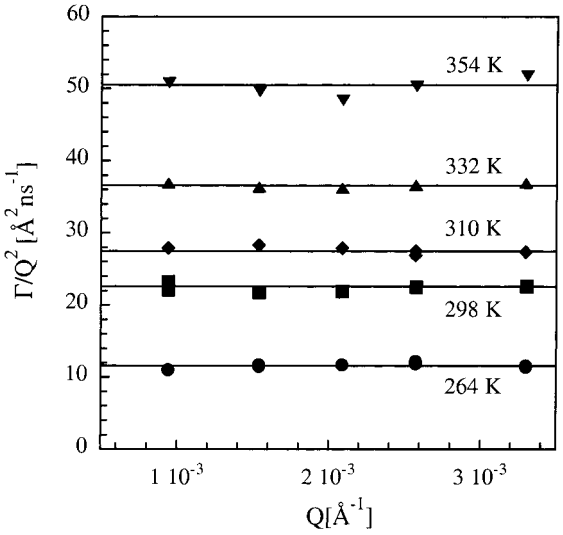

Figure 2. Q dependence of the effective diffusion coefficients obtained for PDMS by DLS at the temperatures indicated for $\phi = 0.07$.

IV. Experimental Results

IV.1. Photon Correlation Spectroscopy. Since PIB is isorefractive to toluene, light scattering experiments could only be performed on PDMS solutions. Spectra were taken in a Q range $10^{-3} \le Q \le 3.3 \times 10^{-3}\ Å^{-1}$ covering a temperature range $264 \le T \le 354$ K. Experiments were performed on $\phi = 0.1$, $\phi = 0.07$, and $\phi = 0.02$ solutions. Because of the very weak contrast at $\phi = 0.02$, these experiments however have a limited accuracy.

In all cases a CONTIN[24] analysis was performed revealing only one single relaxation process. To evaluate the proper relaxation rates $\Gamma(Q)$, we applied accumulant analysis. For the $\phi = 0.07$ sample, Figure 2 displays the obtained Q-dependent effective diffusion coefficients $D_{eff} = \Gamma(Q)/Q^2$ vs Q. In all cases within experimental

Table 2. Temperature Dependence of the Toluene Viscosity η_{tol} and the Effective Diffusion Coefficients Obtained from DLS D_{DLS} and from the Low-Q NSE Spectra D_{NSE} for the Concentrations ϕ Indicated

T (K)	η_{tol} (cP)	D_{DLS} (Å²/ns) $\phi = 0.1$	D_{DLS} (Å²/ns) $\phi = 0.07$	D_{DLS} (Å²/ns) $\phi = 0.02$	D_{NSE} (Å²/ns) $\phi = 0.1$
251	1.07				9.5 ± 0.3
264	0.88	11.3 ± 0.5	11.6 ± 0.4	12.0 ± 0.9	
298	0.56	22.4 ± 1.2	22.6 ± 0.6		
300	0.54				25.9 ± 0.8
310	0.49	28.9 ± 1.1	27.5 ± 0.5	27.8 ± 2.5	
325	0.42	35.6 ± 3.6			
327	0.41				38.5 ± 1.3
332	0.39		36.6 ± 0.3		
343	0.35	45.1 ± 2.1			
354	0.32	53.9 ± 2.4	50.5 ± 1.3	51.0 ± 8.6	
378	0.27				74.1 ± 2.6

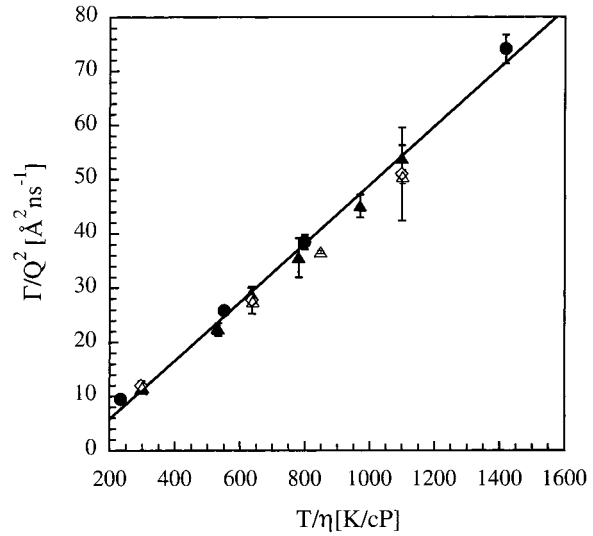

Figure 3. Decay rate Γ divided by Q^2 for PDMS in toluene solution vs the reduced variable T/η. Results correspond to NSE measurements $\phi = 0.1$ (●) and DLS for $\phi = 0.1$ (▲), $\phi = 0.07$ (△), and $\phi = 0.02$ (◇). Solid line shows a linear regression fit of the $\phi = 0.1$ NSE and DLS data.

uncertainty the experimental line widths follow well the expected Q^2 dependence, revealing directly the collective diffusion coefficients. The obtained results are given in Table 2.

The experiments on the $\phi = 0.02$ sample were much more difficult, and even though long measurement times were employed, the experimental errors remained large. Since the contrast diminishes with increasing temperature, the error bars grow at higher T. Table 2 also includes the corresponding results. Comparing the sets of data corresponding to the three concentrations investigated, no concentration dependence of $D(\phi)$ could be detected within the experimental accuracy.

For the PDMS sample the overlap volume fraction amounts to $\phi^* = 0.23$. Both experiments are well below this limit, and since no ϕ dependence was seen, the data may be directly compared with the Zimm prediction[25] for dilute solutions

$$D_Z = 0.196(0.203)\frac{k_B T}{\eta R_e} \qquad (10)$$

where the two coefficients in front are valid for θ and (good) solvents (cgs units). Figure 3 displays the dependence of $D(\phi)$ on T/η. In accordance with eq 10 a very

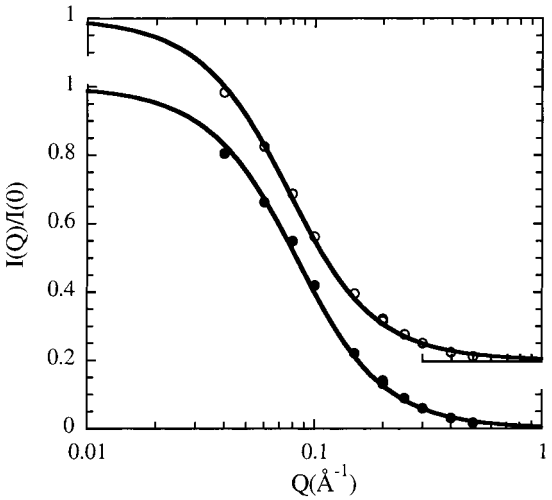

Figure 4. Chain structure factor of PDMS at 251 K (○) and PIB at 268 K (●). Solid lines show the Debye functions corresponding to the ideal chain radii predicted from melt experiments.

good linear relationship is observed. A comparison of the absolute values with eq 10 is done best by looking on the slope of $D(\phi)$ vs T/η in Figure 3. Using $R_e = 52.2$ Å (mean value in the explored temperature range, see later), eq 10 predicts a slope of 5.37×10^{-11} dyn/K, which agrees very well with the measured value of 5.4×10^{-11} dyn/K.

IV.2. Polymer Form Factors. Without the echo configuration in operation, with a NSE spectrometer the degree of polarization of the scattered neutrons may be measured. This mode of operation was used in order to obtain information on the form factors and thereby on the radii of gyration of PIB and PDMS in toluene. To avoid the influence of the virial coefficients, temperatures close to the respective θ-temperatures of both polymers (PIB, $\theta = 260$ K; PDMS, $\theta = 240$ K) were chosen.

The intensity of scattered neutrons not performing a spin flip in the sample is given by $I_u = I_{coh} + {}^1/_3 I_{inc}$ while the spin flip scattering reveals $I_d = {}^2/_3 I_{inc}$, where I_{coh} and I_{inc} are the coherent and incoherent scattering intensities from the sample.[26] Thus, $I_u - {}^1/_2 I_d$ gives the pure coherent scattering. Figure 4 displays the thus obtained form factors for PIB and PDMS at 268 and 251 K, respectively. In the plot the intensities have been normalized to 1 for $Q \to 0$. As expected, both polymers are of very similar size exhibiting nearly identical form factors. The solid lines represent a comparison with Debye form factors (eq 9). There we have taken the radii of gyration from the prediction for ideal chains in melts[27] [$(R_g^{PDMS})^2_{251K} = {}^1/_6(0.408 M_w) \to R_g^{PDMS} = 21$ Å at 251 K and $(R_g^{PIB})^2 = {}^1/_6(0.57 M_w) \to R_g^{PIB} = 19.2$ Å]. Both data sets are well compatible with the melt results.

IV.3. Rouse Dynamics in the Melt. The idea of the experimental approach, namely to learn about the intrachain viscosity of PIB in solution by comparing PIB with PDMS in the regime of intrachain dynamics, rests on the assumption that PDMS having little internal barriers should display "ideal behavior". That this is indeed the case may be realized from a study of the corresponding melt dynamics which is much more straightforwardly evaluated than the solutions.

For this reason we investigated the PDMS sample also in the melt, where the protonated material ($\phi = 0.15$) was immersed in a deuterated melt of identical

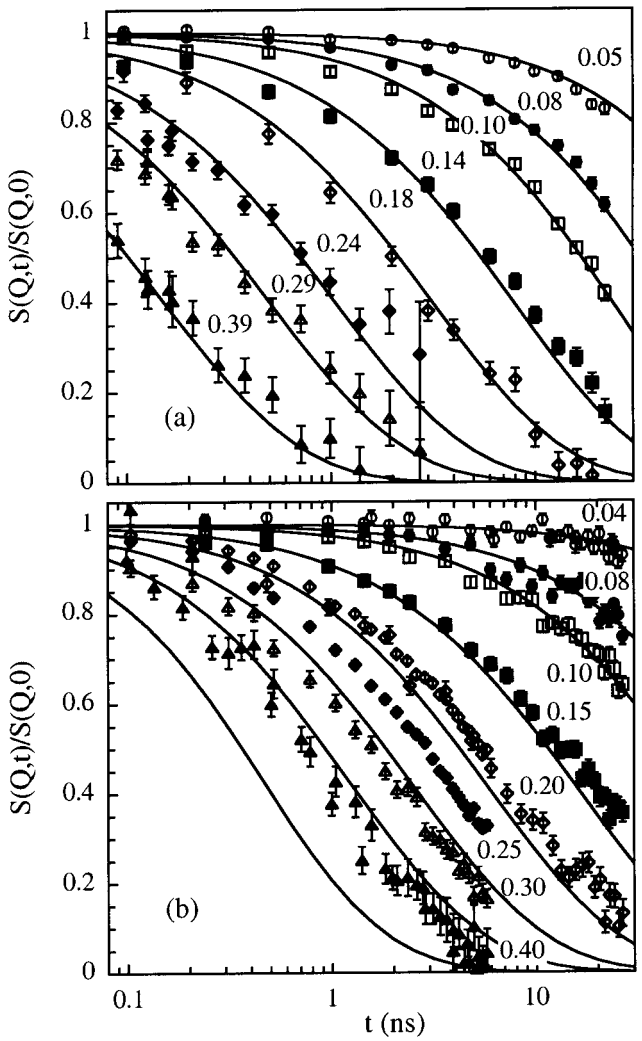

Figure 5. Chain dynamic structure factor of (a) PDMS at 373 K and (b) PIB at 417 K measured in the melt. Each symbol corresponds to the same or very close values of Q for both polymers, which are indicated in the figures. Solid lines show the Rouse prediction.

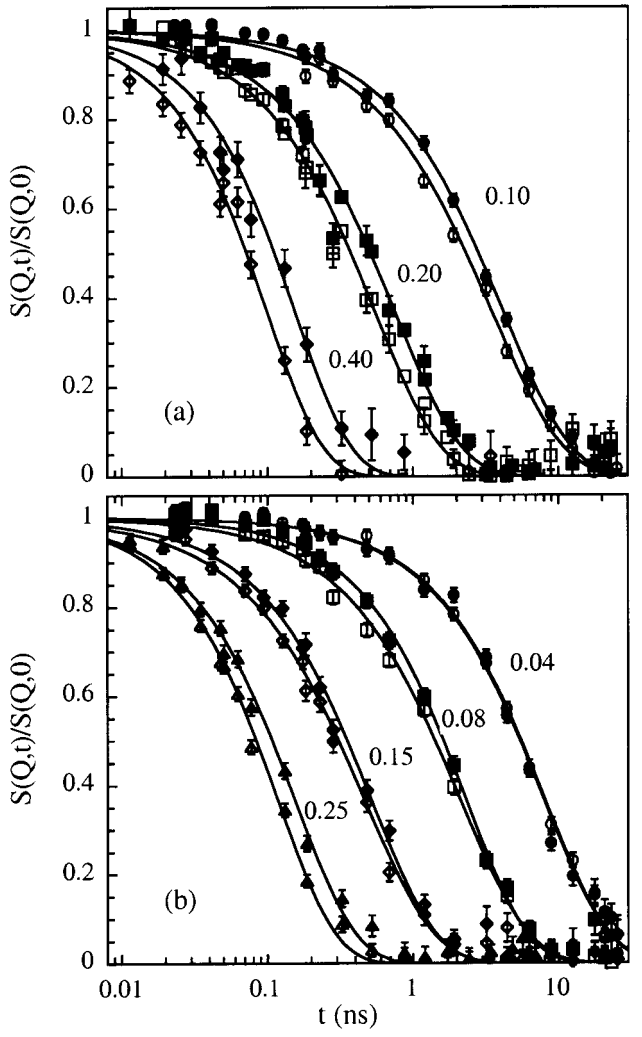

Figure 6. Chain dynamic structure factor of PDMS (empty symbols) and PIB (full symbols) in toluene solution at 300 K (a) and 378 K (b). The corresponding Q values are indicated. Lines through the points are guides to eye.

molecular weight. Figure 5 compares NSE-spectra taken from the PDMS melt at 373 K with spectra from PIB melts (again the same material as used for the solution study) at 417 K. Both sets of spectra are compared with the prediction of the Rouse model (eqs 2, 4, and 5) with $C(q) = C_\infty$ and the draining parameter $B = 0$.

We make two remarks: (i) In an earlier study on PIB[6] we noticed that employing a q-dependent characteristic ratio appropriate for the flexibility of PIB had no influence on the calculated spectra. Therefore, we have omitted any q-dependencies of C_∞. (ii) Any comparison of experimental spectra with the Rouse model requires a consistent incorporation of the Rouse diffusion coefficient $D_R = k_BT/(N\zeta)$ into the description. In the Rouse model D_R and R_g determine all internal relaxation rates. They base on the longest relaxation time $\tau_R = R_g^2/(18\pi^2 D_R)$ which may be related to D_R and R_g only.

In this spirit the experimental spectra for $Q \leq 0.15$ Å^{-1} were fitted with the Rouse model.[3] The solid lines in Figure 5 at higher Q present the Rouse predictions for internal dynamics following from the long-range behavior. For PDMS good agreement with the Rouse model is obtained over the entire accessible Q range, indicating the absence of any important intrachain friction process. The value obtained for the only fitting parameter D_R is $D_R = 2.7$ Å^2/ns. For PIB, on the other hand, beyond $Q \geq 0.15$ Å^{-1} significant deviations appear which grow with increasing Q. At $Q = 0.4$ Å^{-1}; e.g., the data nearly coincide with the prediction for $Q = 0.3$ Å^{-1}. Given the Q^4 dependence of the intrachain relaxation in the Rouse model, this shift signifies a strong slowing down by a factor of the order of $(0.4/0.3)^4 \cong 3$. As we have shown earlier, this effect may be related to intrachain friction as proposed by Allegra et al.

We conclude that PDMS in the experimental Q range displays universal relaxation behavior not yet influenced by intrachain processes or stiffness effects. It therefore may serve as a good basis for a comparison with PIB also in solution, where deviations from the universal behaviors are sought.

IV.4. Spin-Echo Results on the Solutions. All experiments on the polymer solutions were performed at a polymer volume fraction of $\phi = 0.1$. The respective temperature ranges were limited by the neighborhood of the toluene boiling point at the high-temperature side and the respective θ-points of the polymer solutions at the low side. Figure 6 presents typical spectra taken on both polymer solutions at 300 K (a) and 378 K (b). The PDMS data are represented by open symbols, while the PIB data are shown by full symbols. Let us first look

Table 3. Relaxation Rates Obtained for Both Polymers in Toluene Solution ($\phi = 0.1$) by NSE

Q (Å^{-1})	Γ^{PDMS}_{251K} (ns^{-1})	Γ^{PDMS}_{300K} (ns^{-1})	Γ^{PDMS}_{327K} (ns^{-1})	Γ^{PDMS}_{378K} (ns^{-1})	Γ^{PDMS}_{268K} (ns^{-1})	Γ^{PDMS}_{300K} (ns^{-1})	Γ^{PDMS}_{327K} (ns^{-1})	Γ^{PDMS}_{362K} (ns^{-1})	Γ^{PDMS}_{378K} (ns^{-1})
0.04	63.62	22.72	15.62	8.06	52.37	25.42	16.64	10.03	7.92
0.06	30.93	11.23	7.76	4.023	25.93	13.08	8.03	4.89	4.00
0.08	16.09	6.16	3.94	2.06	14.46	7.20	4.23	2.80	2.34
0.10	9.03	3.42	2.27	1.20	8.56	4.15	2.70	1.75	1.37
0.15	3.03	1.14	0.77	0.44	3.06	1.62	1.04	0.60	0.51
0.20	1.30	0.54	0.38	0.22	1.46	0.74	0.47	0.31	0.26
0.25	0.80	0.31	0.22	0.12	0.89	0.44	0.27	0.18	0.16
0.30	0.53	0.21	0.15	0.080	0.61	0.32	0.19	0.12	0.10
0.40	0.35	0.10	0.076	0.044	0.30	0.17	0.10	0.067	0.056

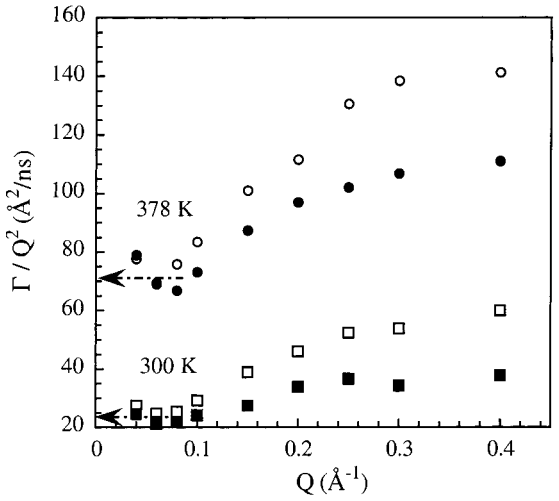

Figure 7. Q dependence of the decay rate Γ divided by Q^2 for PDMS (empty symbols) and PIB (full symbols) in solution. Squares correspond to 300 K and circles to 378 K. The dashed arrows show the values obtained by DLS for PDMS.

at the data at 378 K. At $Q = 0.04$ Å^{-1} ($QR_g \cong 0.8$) we are in the regime of translational diffusion, where the contributions of the intrachain modes amount to ≈1% only. There the spectra from both polymers are identical. Since both polymers are characterized by equal chain dimensions, the equality of the translational diffusion coefficients implies that also the draining properties are equal. In going now to larger Q values, gradually the spectra from the PIB solutions commence to decay at later times. This effect increases with increasing Q and is maximal at $Q = 0.4$ Å^{-1} in Figure 6a.

To perform a line shape analysis, we fitted the spectra with a stretched exponential relaxation function $\sim \exp\{-[t\Gamma(Q)]^{\beta}\}$. For all spectra the shapes turned out to be close to a single exponential ($0.9 \leq \beta \leq 1$). To get to easily comparable decay rates, we therefore fitted subsequently all spectra with a Debye relaxation ($\beta = 1$). The obtained relaxation rates are given in Table 3. Figure 7 compares the effective diffusion coefficients $\Gamma(Q)/Q^2 = D_{eff}$ from both polymers for two different temperatures. Again, we realize the close agreement of the corresponding D_{eff} from both polymers in the low Q regime. At higher Q, on the other hand, where we are in the regime of the internal chain relaxations, significant differences are visible. Thus, without any sophisticated data evaluation, just from a qualitative inspection of the results the retardation of the intrachain relaxation in PIB compared to PDMS reveals itself. At larger Q, D_{eff} in PIB is reduced by about 50% at 300 K and by around 30% at 378 K. The effect is weaker than in the melt, where reductions by factors of 3 are found, but still significant.

By a dashed line Figure 7 also includes the collective diffusion coefficients found by light scattering. The lines go through the middle of the spread of the NSE low Q results and are in good quantitative agreement with the neutron data which were obtained at 1.5 order of magnitude larger Q values. For a quantitative comparison we have included the average of the three lowest Q (0.04, 0.06, and 0.08 Å^{-1}) effective diffusion coefficients from NSE into Table 2 and find excellent agreement with light scattering.

For the quantitative evaluation of the intrachain modes the translational diffusion coefficients of both polymers need to be well-known. Collecting the experimental findings, we observed that (i) the PDMS light scattering diffusion coefficients within the experimental errors were independent of polymer concentration, i.e., they are also representative for the self-diffusion coefficients at least at high dilution; (ii) the light scattering data agree very well with the neutron results at much higher Q. Thus, the diffusion coefficients are not significantly Q-dependent; (iii) the PIB and PDMS diffusion coefficients in the neutron range agree nearly quantitatively (see Table 3 and Figure 7).

For PIB light scattering data are not available. Given the experimental coincidences above together with the identical dimensions of both polymers, it is well justified in both cases to take the average neutron effective diffusion coefficients as a basis for the further evaluation of the NSE spectra at higher Q.

V. Analysis and Discussion

V.1. Zimm Analysis of the PDMS Solution Results. The PDMS and the PIB chains consist of around 78 monomers, rendering the usual applied long wavelength approximation ($\tau_p^{-1} \sim p^{3/2}$) of the Zimm model invalid. For such short chains the Rouse−Zimm model needs to be evaluated according to eq 4, where we applied the approximation by the FresnelC function. The data were fitted keeping the translational diffusion coefficient fixed as discussed in section IV.5. The draining parameter $B = (\sqrt{6/\pi})(b/l\sqrt{C_\infty})$ served as the only fitting parameter [$C(q) \equiv C_\infty$]. With this approach an excellent description of all spectra is reached. As a representative result, Figure 8a displays the obtained fit for $T = 327$ K.

In these fits the hydrodynamic interaction is captured by the draining parameter. Depending on temperature values for B between 0.38 (251 K) and 0.30 (378 K) are found (all values are in Table 4). Compared to NSE results on long PDMS chains, these B values are low. For example, for PDMS ($M_w = 60\,000$) in the θ-solvent bromobenzene at 357 K $B = 0.60$ was found.[2] Experiments in toluene gave $B \approx 0.50$ at 373 K.[2] In particular, a comparison with the earlier study of long chains in

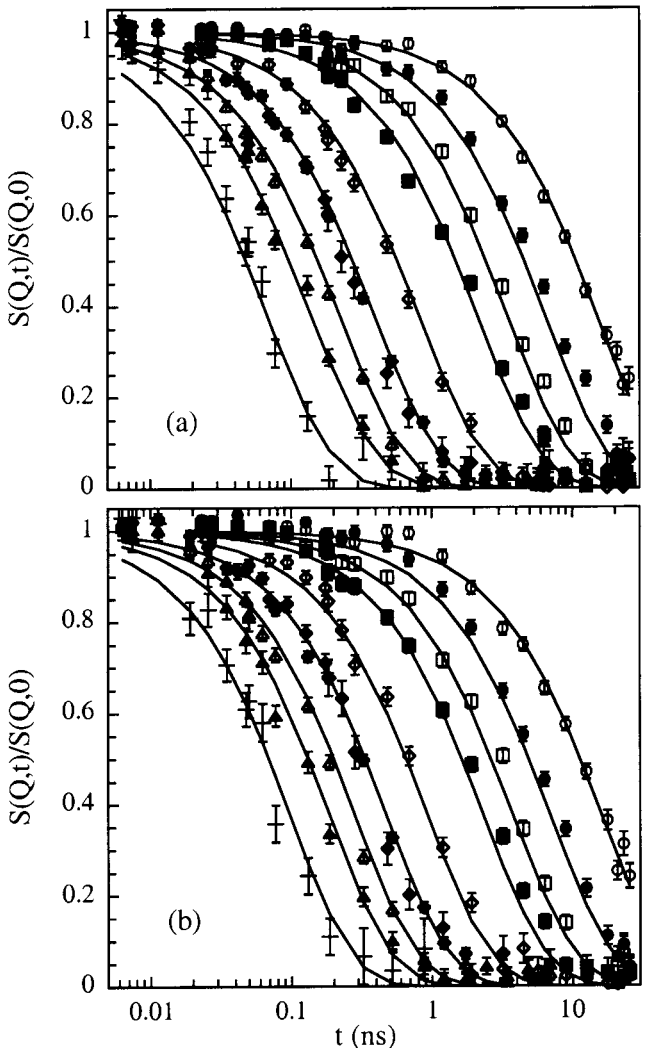

Figure 8. Chain dynamic structure factor of PDMS (a) and PIB (b) in toluene solution at 327 K at the Q values: 0.04 Å^{-1} (○); 0.06 Å^{-1} (●); 0.08 Å^{-1} (□); 0.10 Å^{-1} (■); 0.15 Å^{-1} (◇); 0.20 Å^{-1} (◆); 0.25 Å^{-1} (△); 0.30 Å^{-1} (▲); 0.40 Å^{-1} (+). Solid lines correspond to fitting curves: Rouse−Zimm model for PDMS and Rouse−Zimm with intrachain viscosity for PIB (see text).

Table 4. Temperature Dependence of the Draining Parameter B Obtained for PDMS Chains and the Characteristic Time τ_0 Deduced for PIB

T (K)	B	τ_0 (ns)
251	0.38 ± 0.02	
268		0.427 ± 0.012
300	0.36 ± 0.01	0.230 ± 0.008
327	0.34 ± 0.01	0.138 ± 0.006
362		0.098 ± 0.005
378	0.30 ± 0.04	0.095 ± 0.005

toluene at 373 K with our results at 378 K shows that the observed small draining parameters seem to be a chain length effect: since the hydrodynamic flow field decays only weakly with distance ($1/r$), the development of full draining behavior appears to need a large number of monomers within a chain.[28]

V.2. Intrachain Viscosity Analysis of the PIB Data. The Allegra approach[4,5] bases on the physical idea of an intrachain viscous resistance to configurational equilibration after an excursion from equilibrium. In solution the corresponding relaxation time should relate to jumps across the rotational barriers within the chain. For the PIB analysis we took the results of the Rouse−Zimm evaluation of PDMS as an input; i.e., we performed the analysis with the full solution of the Allegra model fixing the draining parameters to the PDMS values. Figure 8b displays the results of such a fit at 327 K with τ_0 being the only fit parameter—the diffusion coefficient again was extracted from the low Q results and kept fixed (see section IV.5). We achieved very good fits at all temperatures. The resulting values for τ_0 are given in Table 4 and displayed in Figure 9. $\tau_0(T)$ follows an activated behavior with an activation energy E = 3.1 ± 0.3 kcal/mol,

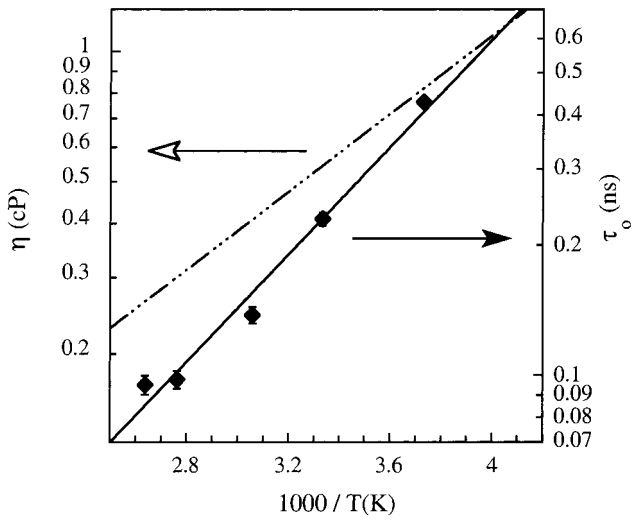

Figure 9. T dependence of the solvent viscosity (dashed line) and the characteristic time τ_0 deduced for the conformational transitions in PIB (◆). The solid line through the points corresponds to the fit to an Arrhenius law.

$$\tau_0 = 1.27 \times 10^{-12} \exp\left[\frac{3.1}{RT}\right] \text{[s]} \qquad (11)$$

The preexponential factor of about 1 ps lies well in the microscopic range. The true activation energy might be somewhat higher because all the evaluation was performed relative to PDMS and any rotational barrier of PDMS would have to be added. For comparison, we also display the temperature dependence of the solvent viscosity η_{tol} which is characterized by an activation energy of 2 kcal/mol.

V.3. Discussion. Though NMR experiments in general do not provide space−time resolutions as neutron scattering, in solutions in principle they access the local reorientational motions. PIB in solution has been studied by NMR spin−lattice relaxation by several authors. These experiments measure the activation energy of the spin−lattice relaxation time T_1 which is related to the sum of the activation energy of the local process E_{loc} and that of the viscosity E_η: $E_{T1} = E_{loc} + E_\eta$. From such an evaluation of T_1 experiments Dejean de la Batie et al.[8] found E_{loc} = 5 kcal/mol for PIB in chloroform, while Jones et al.[9] and Inoue et al.[10] observed 4.3 and 3.6 kcal/mol, respectively.

On the theoretical side the RIS (rotational−isomeric state) calculations of Suter et al.[11] employed activation energies of 3−4 kcal/mol, while the molecular dynamics simulations of Vacatello and Yoon[12] based on a rotational barrier of 2.8 kcal/mol.

This data array fits the upper range of the rotational barriers of the hydrocarbons which are found typically between 3 ≤ E ≤ 3.5 kcal/mol. The value of 3.1 kcal/mol for the activation energy of τ_0 resulting from the intrachain viscosity analysis of our PIB/toluene data is

well in this range and allows us to identify the mechanism behind the intrachain friction as rotational jumps which change chain conformation. The finding corroborates the physical picture behind the Allegra mechanism and shows that the intrachain viscosity appears to be the leading mechanism causing deviations from universal relaxation in going to local scales.

For the case of polymer solutions our experiments have clearly demonstrated that the basic process which limits the validity of the universal Zimm relaxation locally relates to conformational rearrangements in terms of crossing rotational barriers. As we have shown earlier, in the melt the same mechanism is active, though the relation between the observed activation energy and the barrier height for a single intrachain rotational motion is not clear. Nevertheless, from the comparison between the melt dynamics of PDMS and PIB it is clear that, at least for flexible chains, the local stiffness models[29] do not apply. These models assume the chain rigidity to be the leading mechanism causing deviations from the Rouse model at more local scales. PDMS and PIB exhibit very similar characteristic ratios ($C_\infty^{\mathrm{PDMS}} = 6.19$, $C_\infty^{\mathrm{PIB}} = 6.73$). Thus, the local static chain stiffness which gives rise to the overall chain dimension is practically equal for both chains. Any model that assigns the chain rigidity to be the major source for the deviations from Rouse relaxation toward local scales would necessarily have to consider PDMS and PIB as similar. Our comparative study of the melt dynamics of both polymers shows, however, that they exhibit different dynamic structure factors. While for PDMS the Rouse model holds up to $Q = 0.4$ Å^{-1}, in PIB strong deviations are building up starting beyond $Q = 0.15$ Å^{-1}. Thus, not bending stiffness but rotational dynamics limits the universal relaxation schemed in flexible polymers toward local scales.

Finally, we remark on the observed diffusion behavior of PDMS which we consider as somewhat surprising. In sections 3 and 4 we reported the observation of a concentration- and Q-independent diffusion coefficient at least within the experimental uncertainties. On the other hand, the second virial coefficient of PDMS in toluene for our molecular weight amounts[30] to about $(8-9) \times 10^{-4}$ cm^{-3} which according to eq 8 should induce a strong increase of $D(\phi)$ with ϕ. Seemingly the effect must be counterbalanced by an equally strong hydrodynamic factor k_s^ϕ. In that case $D(\phi) \cong D(\phi{=}0) = D_{\mathrm{self}}(0)$. This raises the question of the Q dependence of the various diffusion coefficients. With increasing Q the collective diffusion coefficient should approach the self-diffusion coefficient. Following eq 9 the corresponding length scale is set by the radius of gyration. The Q dependence of the self-diffusion coefficient is not clear, but one would expect that at local scales, where the polymer does not yet realize the cage set by the surrounding coils, the self-diffusion coefficient should equal the value at infinite dilution. Our data are not sufficient to make any clear statement, but the systematic Q dependence of $\Gamma(Q)/Q^2$ at low Q, where always a slight minimum around $Q = 0.08$ Å^{-1} is observed (see Figure 7), may indicate the combined effect of decreasing collective and increasing self-diffusion coefficients. Here future Q-dependent experiments would be interesting. We note that our evaluation scheme for the intrachain modes would not be affected by such diffusional crossovers. In the intrachain regime $D_{\mathrm{self}}(\phi{=}0)$ would hold which within the experimental precision equals $D(\phi{=}0.1)$.

VI. Conclusions

In a previous paper,[6] we have shown that in polymer melts the leading mechanism behind the deviations from Rouse relaxation toward local scales can be associated with an internal viscosity effect as proposed by Allegra et al.[4,5] Now in studying solutions the present work aimed on a quantitative identification of the process to see whether the physical picture of a delayed redistribution of conformational states ruling internal viscosity applies. For this purpose a comparative study on PDMS—a polymer without or very little internal barriers[13]—and PIB—a high barrier hydrocarbon[8−12]—was undertaken. We found the following:

(i) The melt dynamics of PDMS can be described up to $Q = 0.4$ Å^{-1} in terms of the Rouse model with no signs of intrachain friction, qualifying this polymer as an ideal reference system.

(ii) In solution the collective diffusion coefficient of PDMS is largely Q- and concentration-independent.

(iii) The intrachain dynamics of PDMS may be well described with the Rouse−Zimm model. For the short investigated chain the draining parameter is significantly lower than for corresponding long chain PDMS solutions.

(iv) Using the PDMS results as an input, PIB data from a chain with identical size and diffusion coefficients as PDMS were analyzed in terms of the full solution of the internal viscosity model of Allegra et al.

(v) The resulting delay time τ_0 causing the internal viscosity effect exhibits an activation energy typical for single rotational barriers in PIB.

Comparing PIB and PDMS relaxation in the melt led to the conclusion that, given identical static rigidity, the different dynamics must relate to an intrachain relaxation process. Then the solution data clearly demonstrate that (1) the internal viscosity model of Allegra et al. is able to quantitatively describe all solution results and (2) the relaxation mechanism behind the internal viscosity effect is indeed the jump across rotational barriers.

Acknowledgment. We thank Prof. Colmenero for fruitful discussions. A.A. acknowledges support from the following projects: DGICYT, PB97-0638; GV, EX 1998-23; UPV/EHU, 206.215-G20/98. Support from "Donostia International Physics Center" is also acknowledged.

References and Notes

(1) Doi, M.; Edwards, S. F. In *The Theory of Polymer Dynamics*; Clarendon: Oxford, 1986.
(2) Ewen, B.; Richter, D. In *Advances in Polymer Science*; Springer-Verlag: Berlin, Heidelberg, 1997; Vol. 134.
(3) Rouse, P. E., Jr. *J. Chem. Phys.* **1953**, *21*, 1272.
(4) Allegra, G.; Ganazzoli, F. *Macromolecules* **1981**, *14*, 1110.
(5) Allegra, G.; Ganazzoli, F. In *Advances in Chemical Physics*; Prigogine, I., Rice, S. A., Eds.; Wiley: New York, 1989; Vol. 75, p 265.
(6) Richter, D.; Monkenbusch, M.; Allgeier, J.; Arbe, A.; Colmenero, J.; Farago, B.; Cheol Bae, Y.; Faust, R. *J. Chem. Phys.* **1999**, *111*, 6107.
(7) Yamakawa, H. In *Modern Theory of Polymer Solutions*; Harper & Row: New York, 1971.
(8) Dejean de la Batie, R.; Lauprêtre, F.; Monnerie, L. *Macromolecules* **1989**, *22*, 2617.
(9) Jones, A. A.; Lubianez, R. P.; Hanson, M. A.; Shostak, S. L. *J. Polym. Sci., Polym. Phys. Ed.* **1978**, *16*, 1685.
(10) Inoue, Y.; Nishioka, A.; Chûjô, R. *J. Polym. Sci., Polym. Phys. Ed.* **1973**, *11*, 2237.
(11) Suter, U. W.; Saiz, E.; Flory, P. J. *Macromolecules* **1983**, *16*, 1317.

(12) Vacatello, M.; Yoon, D. Y. *Macromolecules* **1992**, *25*, 2502.
(13) Bahar, I.; Zuniga, I.; Dodge, R.; Mattice, W. L. *Macromolecules* **1991**, *24*, 2986.
(14) Brückner, S. *Macromolecules* **1981**, *14*, 449.
(15) Flory, P. J. *Statistical Mechanics of Chain Molecules*; Interscience: New York, 1969.
(16) Brown, W.; Zhou, P. *Macromolecules* **1991**, *24*, 5151.
(17) Cotts, P. M.; Selser, J. C. *Macromolecules* **1990**, *23*, 2050.
(18) de Gennes, P. G. *Physica* **1959**, *25*, 825.
(19) Ndoni, S.; Papadakis, C. M.; Bates, F. S.; Almdal, K. *Rev. Sci. Instrum.* **1995**, *66*, 1090.
(20) Almdal, K., manuscript in preparation.
(21) *CRC Handbook of Chemistry and Physics*; Lide, D. L., Ed.; CRC Press: New York, 1999.
(22) See, e.g.: Berne, B. J.; Pecora, R. *Dynamic Light Scattering*; John Wiley & Sons: New York, 1976.
(23) See, e.g.: *Neutron Spin Echo*; Mezei, F., Ed.; Lecture Notes in Physics; Springer-Verlag: Heidelberg, 1980; Vol. 28.
(24) Provencher, S. W. *Comput. Phys. Commun.* **1982**, *27*, 213.
(25) Zimm, B. H. *J. Chem. Phys.* **1956**, *24*, 269.
(26) Marshall, W.; Lovesey, S. W. In *Theory of Thermal Neutron Scattering*; Oxford University Press: Oxford, 1971.
(27) Fetters, L. J.; Lohse, D. J.; Richter, D.; Witten, T. A.; Zirkel, A. *Macromolecules* **1994**, *27*, 4639.
(28) Edwards, C. J. C.; Stepto, R. F. T.; Semlyen, J. A. *Polymer* **1982**, *23*, 865.
(29) Harnau, L.; Winkler, R. G.; Reineker, P. *J. Chem. Phys.* **1995**, *102*, 7750; **1996**, *104*, 6355.
(30) *Polymer Handbook*; Brandrup, J., Immergut, E. H., Grulke, E. A., Eds.; John Wiley and Sons: New York, 1999.

MA001628X